Broadband hitless silicon electro-optic switch for on-chip optical networks

Hugo L. R. Lira, Sasikanth Manipatruni, and Michal Lipson*

School of Electrical and Computer Engineering, Cornell University, Ithaca, NY 14853, U.S.A.
**ml292@cornell.edu*

Abstract: We report on the demonstration of a broadband (60 GHz), spectrally hitless, compact (20 μm x 40 μm), fast (7 ns) electro-optical switch. The device is composed of two coupled resonant cavities, each with an independently addressable PIN diode. This topology enables operation of the switch without perturbing adjacent channels in a wavelength division multiplexing (WDM) system.

OCIS codes: (250.3140) Integrated optoelectronic circuits; (250.6715) Switching; (230.4555) Coupled resonators; (230.3120) Integrated optics devices.

References and links

1. A. Shacham, K. Bergman, and L. P. Carloni, "On the Design of a Photonic Network-on-Chip," in *Proceedings of IEEE International Symposium on Networks-on-Chips* (IEEE, 2007), pp. 53–64.
2. C. Batten, A. Joshi, J. Orcutt, A. Khilo, B. Moss, C. Holzwarth, M. Popovic, H. Li, H. Smith, J. Hoyt, F. Kartner, R. Ram, V. Stojanovic, and K. Asanovic, "Building Manycore Processor-to-DRAM Networks with Monolithic Silicon Photonics," in *16th IEEE Symposium on High Performance Interconnects, 2008. HOTI '08*, 21–30, 26–28 Aug. 2008.
3. International Technology Roadmap for Semiconductors, (ITRS 2007) *http://www.itrs.net/Links/2007ITRS/2007_Chapters/2007_Interconnect.pdf*.
4. A. W. Poon, X. Luo, F. Xu, and H. Chen, "Cascaded microresonator-based matrix switch for silicon on-chip optical interconnection," Proc. IEEE **97**(7), 1216–1238 (2009).
5. B. G. Lee, B. A. Small, K. Bergman, Q. Xu, and M. Lipson, "Transmission of high-data-rate optical signals through a micrometer-scale silicon ring resonator," Opt. Lett. **31**(18), 2701–2703 (2006).
6. F. J. Mesa-Martinez, M. Brown, J. Nayfach-Battilana, and J. Renau, "Measuring performance, power, and temperature from real processors," in *Proc. of the 2007 Workshop on Experimental Computer Science*, San Diego, CA, Jun. 13 - 14, 2007. ExpCS '07. ACM, New York, NY.
7. Y. Goebuchi, T. Ka, and Y. Kokubun, "Fast and Stable Wavelength-Selective Switch Using Double-Series Coupled Dielectric Microring Resonator," IEEE Photon. Technol. Lett. **18**(3), 538–540 (2006).
8. Y. Goebuchi, M. Hisada, T. Kato, and Y. Kokubun, "Optical cross-connect circuit using hitless wavelength selective switch," Opt. Express **16**(2), 535–548 (2008).
9. M. A. Popović, T. Barwicz, F. Gan, M. S. Dahlem, C. W. Holzwarth, P. T. Rakich, H. I. Smith, E. P. Ippen, and F. X. Kärtner, "Transparent wavelength switching of resonant filters," presented at Conference on Lasers and Electro-Optics (CLEO), Baltimore, MD, May 10, 2007, postdeadline paper CPDA2.
10. Y. Vlasov, W. M. J. Green, and F. Xia, "High-throughput silicon nanophotonic wavelength-insensitive switch for on-chip optical networks," Nat. Photonics **2**(4), 242–246 (2008).
11. H. A. Haus, M. A. Popović, and M. R. Watts, "Broadband Hitless Bypass Switch for Integrated Photonic Circuits," IEEE Photon. Technol. Lett. **18**(10), 1137–1139 (2006).
12. S. Y. Cho, and R. Soref, "Interferometric microring-resonant 2 x 2 optical switches," Opt. Express **16**(17), 13304–13314 (2008).
13. M. Watts, D. C. Trotter, and R. W. Young, "Maximally Confined High-Speed Second-Order Silicon Microdisk Switches," in *National Fiber Optic Engineers Conference*, OSA Technical Digest (CD) (Optical Society of America, 2008), paper PDP14.
14. C. Li, X. Luo, and A. W. Poon, "Dual-microring-resonator electro-optic logic switches on a silicon chip," Semicond. Sci. Technol. **23**(6), 064010 (2008).
15. S. Manipatruni, Q. Xu, B. Schmidt, J. Shakya, and M. Lipson, "High Speed Carrier Injection 18 Gb/s Silicon Micro-ring Electro-optic Modulator," in *The 20th Annual Meeting of the IEEE Lasers and Electro-Optics Society* (IEEE, 2007), p. 537.
16. M. W. Geis, S. J. Spector, R. C. Williamson, and T. M. Lyszczarz, "Submicrosecond Submilliwatt Silicon-on-Insulator Thermooptic Switch," IEEE Photon. Technol. Lett. **16**(11), 2514–2516 (2004).
17. R. Orta, P. Savi, R. Tascone, and D. Trinchero, "Synthesis of Multiple-Ring-Resonator Filters for Optical Systems," IEEE Photon. Technol. Lett. **7**(12), 1447–1449 (1995).

#117101 - $15.00 USD Received 11 Sep 2009; revised 12 Nov 2009; accepted 16 Nov 2009; published 23 Nov 2009

18. B. E. Little, S. T. Chu, H. A. Haus, J. Foresi, and J.-P. Laine, "Microring Resonator Channel Dropping Filters," J. Lightwave Technol. **15**(6), 998–1005 (1997).
19. A. Melloni, and M. Martinelli, "Synthesis of Direct-Coupled-Resonators Bandpass Filters for WDM Systems," J. Lightwave Technol. **20**(2), 296–303 (2002).
20. A. Yariv, "Universal relations for coupling of optical power between microresonators and dielectric waveguides," Electron. Lett. **36**(4), 321–322 (2000).
21. J. Poon, J. Scheuer, S. Mookherjea, G. T. Paloczi, Y. Huang, and A. Yariv, "Matrix analysis of microring coupled-resonator optical waveguides," Opt. Express **12**(1), 90–103 (2004).
22. F. Xia, L. Sekaric, and Y. A. Vlasov, "Mode conversion losses in silicon-on-insulator photonic wire based racetrack resonators," Opt. Express **14**(9), 3872–3886 (2006).
23. Q. Xu, B. Schmidt, S. Pradhan, and M. Lipson, "Micrometre-scale silicon electro-optic modulator," Nature **435**(7040), 325–327 (2005).
24. C. Manolatou, and M. Lipson, "All-Optical Silicon Modulators Based on Carrier Injection by Two-Photon Absorption," J. Lightwave Technol. **24**(3), 1433–1439 (2006).
25. Y. P. Varshni, "Temperature dependence of the energy gap in semiconductors," Physica E (Amsterdam) **34**(1), 149–154 (1967).
26. P. Dumon, G. Priem, L. R. Nunes, W. Bogaerts, D. van Thourhout, P. Bienstman, T. K. Liang, M. Tsuchiya, P. Jaenen, S. Beckx, J. Wouters, and R. Baets, "Linear and Nonlinear Nanophotonic Devices Based on Silicon-on-Insulator Wire Waveguides," Jpn. J. Appl. Phys. **45**(No. 8B), 6589–6602 (2006).
27. R. A. Soref, and B. R. Bennett, "Electrooptical Effects in Silicon," IEEE J. Quantum Electron. **23**(1), 123–129 (1987).
28. H. C. Huang, S. Yee, and M. Soma, "Quantum calculations of the change of refractive index due to free carriers in silicon with nonparabolic band structure," J. Appl. Phys. **67**(4), 2033–2039 (1990).
29. J. T. Robinson, K. Preston, O. Painter, and M. Lipson, "First-principle derivation of gain in high-index-contrast waveguides," Opt. Express **16**(21), 16659–16669 (2008).
30. S. Manipatruni, Q. Xu, and M. Lipson, "PINIP based high-speed high-extinction rat**io** micron-size silicon electrooptic modulator," Opt. Express **15**(20), 13035–13042 (2007).
31. J. Van Campenhout, W. M. J. Green, X. Liu, S. Assefa, R. M. Osgood, and Y. A. Vlasov, "Silicon-nitride surface passivation of submicrometer silicon waveguides for low-power optical switches," Opt. Lett. **34**(10), 1534–1536 (2009).

1. Introduction

Optical switches are critical elements for on-chip optical networks. They are essential for high performance interconnects in a multi-core microprocessor system [1,2], where large bandwidth densities, low energy consumption and small footprint components are required [3,4]. Here we demonstrate hitless operation of a broadband compact electro-optic switch for on-chip optical networks on a silicon platform.

A broadband switch is important for two main reasons: low distortion of high bandwidth signals [5], and robustness from on chip temperature changes [6]. Hitless tuning, i.e. switching data at one wavelength without affecting the other wavelengths on the interconnect (see Fig. 1), is also an important criterion in on-chip optical networks employing multiple wavelengths [1]. A broadband hitless switch provides the ability to enable and disable a WDM channel drop filter without blocking an adjacent channel in the network.

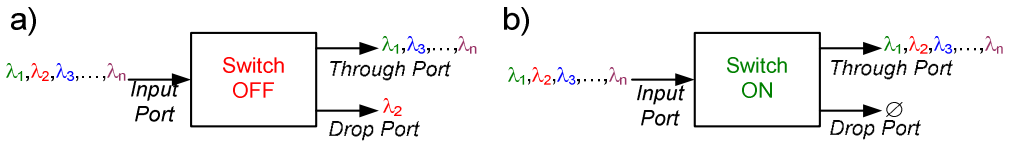

Fig. 1. Hitless switch scheme. a) When the switch is OFF, a single wavelength channel in a WDM system is directed to the drop port. b) When the switch is ON, no channel is dropped.

Previously, thermo-optic [7–9] and all-optical [10] approaches have been used to demonstrate broadband hitless switching using coupled resonators, and also proposed to be used in a Mach-Zehnder topology [11,12]. Electro-optic broadband switching has also been demonstrated, however not in a hitless configuration [13,14]. Here, we show the synthesis procedure, implementation and analysis of a broadband, hitless, compact electro-optic switch on a silicon photonics platform, using a compact broadband filter integrated with PIN diodes [15].

#117101 - $15.00 USD Received 11 Sep 2009; revised 12 Nov 2009; accepted 16 Nov 2009; published 23 Nov 2009

2. Switch description and synthesis

The device analyzed and fabricated consists of two coupled optical cavities surrounded by p-doped and n-doped regions. The two cavities create a broadband transmission while the integrated PIN diodes enable free carrier injection and extraction to change the refractive index of silicon [15]. A schematic of the device with its transfer function for distinct detuning values is shown in Fig. 2.

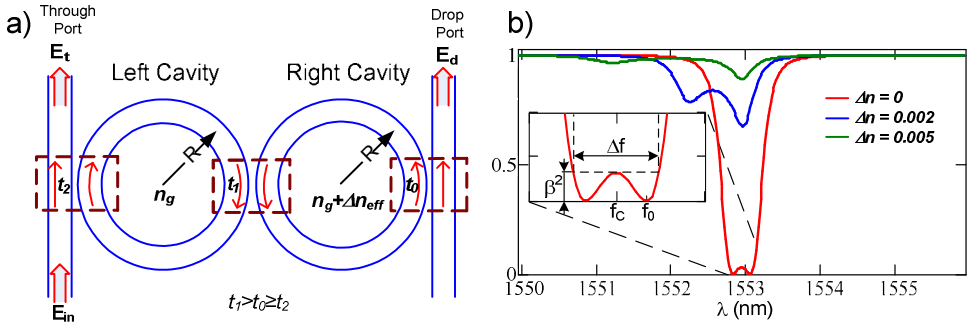

Fig. 2. (a) Schematic of two coupled ring resonators with (b) its theoretical through port transmission spectrum. Red line shows the original transmission where the two cavities share the same resonance. The blue line shows a transient state and green line the final state of the switch, where detuning was provided by changing the refractive index of the right cavity.

The broadband operation of the device is achieved when a) the cavities share the same resonance wavelength and b) the coupling between each cavity and its adjacent waveguide is much stronger than the coupling between cavities. The hitless operation of the switch is achieved by changing the resonance of the cavity coupled to the drop waveguide while leaving the other unperturbed. When both cavities share the same resonance, light with frequency within the filter bandwidth is directed to the drop port. When the index of the cavity coupled to the drop port (right cavity in Fig. 2) is changed, the cavities no longer share the same resonances. This leads to an over-coupled system and the signal is routed to the through port. The fact that the index of the cavity coupled to the through port (left cavity in Fig. 2) is not changed prevents perturbing adjacent channels, which is the goal of a hitless device. In principle, even the residual dispersion caused by the presence of the over-coupled cavity can be reduced by slightly detuning it to the edge of the WDM channel, or to a nearby region between two WDM communication channels,.

The detuning mechanism used for changing the refractive index plays an important role for the possible applications of the device. Changing the refractive index by free carrier dispersion is crucial for systems which require fast switching transitions (a few nanoseconds) of small data packets (sub-microsecond or a few microseconds, depending on the amount of detuning provided, as shown on section 3), once thermo-optical effect caused by the current flowing through the device heats it up and reduces the index change provided by the free carrier dispersion. Thermo-optical detuning, as has been shown in [7–9], is suitable for switching times about hundreds of nanoseconds at best [16], with unlimited holding time.

In order to optimize the device performance we calculate the coupling conditions, i.e., the transmission values for each directional coupler present in the device [t_0, t_1 and t_2 in Fig. 2(a)] as a function of the desired bandwidth (Δf) given a desired intensity attenuation coefficient β^2, also known as power ripple, shown in the inset of Fig. 2(b). General methods for filter synthesis when there is no propagation loss has been extensively studied for CROW systems [17–19]. Here we provide the steps for a Chebyshev-like transfer function implementation when losses are considered in a two ring device, by forcing the minimum transmission to be zero and the maximum to be β^2 inside the bandwidth of the transmission spectrum of the through port.

#117101 - $15.00 USD Received 11 Sep 2009; revised 12 Nov 2009; accepted 16 Nov 2009; published 23 Nov 2009

The equations for the field at the through and drop ports are:

$$E_t = \frac{t_2 - e^{i\phi_2} a_2 E_{t1}}{1 - t_2 e^{i\phi_2} a_2 E_{t1}} \quad \text{and} \quad E_d = \frac{\sqrt{e^{i\phi_2} a_2} \cdot (-ik_2) \cdot E_{d1}}{1 - t_2 e^{i\phi_2} a_2 \cdot E_{t1}} \tag{1}$$

with [20]

$$E_{t1} = \frac{t_1 - e^{i\phi_1} a_1 t_0}{1 - t_1 e^{i\phi_1} a_1 t_0} \quad \text{and} \quad E_{d1} = \frac{-\sqrt{e^{i\phi_1} a_1} \cdot (-ik_1) \cdot (-ik_0)}{1 - t_1 e^{i\phi_1} a_1 t_0} \tag{2}$$

and with

$$a_i = e^{-\frac{\alpha + \Delta\alpha_i}{2} \cdot 2\pi R} \quad \text{and} \quad \phi_i = \frac{2\pi}{\lambda} \cdot \left(n_g + \Delta n_{eff\,i}\right) \cdot 2\pi R \tag{3}$$

where E_t is the field intensity at through port, E_d is the field intensity at drop port, t_0, t_1 and t_2 are the transmission coefficients of the directional couplers shown in Fig. 2(c), k_0, k_1 and k_2 are the coupling coefficients of the directional couplers, R is the radius of the rings, α is intrinsic loss, $\Delta\alpha_i$ is the loss caused by free-carrier absorption, a_i is the roundtrip attenuation coefficient for ring i, n_g is the group index of the device, $\Delta n_{eff\,i}$ is the refractive index change caused by free-carrier dispersion for ring i, and λ is the free space wavelength. With no free-carrier injection the values for roundtrip attenuation coefficient are equal $a_1 = a_2 = a$ and phases are also equal $\phi_1 = \phi_2 = \phi$. The equations are shown in a recursive fashion and can be easily extended for higher order filters, although a matrix analysis method can also be used [21]. Analogous to the condition for critical coupling in a single ring [20], critical coupling for two rings requires that the transmission in the input waveguide is equal to the product of attenuation coefficients and transmission coefficient of the output waveguide:

$$t_2 = a^2 t_0 \tag{4}$$

Plugging Eq. (4) into the equation for the transmission field E_t and forcing it to have zeros in the numerator we obtain:

$$t_1 = \cos\phi_0 \frac{2a \cdot t_0}{1 + t_0^{\,2} a^2} \tag{5}$$

where ϕ_0 is the value of the phase ϕ that provides zeros in the through port transmission spectrum. Plugging Eq. (4) and Eq. (5) in Eq. (1) and considering that the minimum attenuation allowed inside the bandwidth (β) happens for $\phi = 0$, the following equation is obtained for t_0:

$$(a \cdot t_0)^4 - 2\frac{(1 - \cos\phi_0)}{\beta \cdot a}(a \cdot t_0)^3 - \frac{(a^2 + 1)(2 \cdot \cos\phi_0 - 1)}{a^2}(a \cdot t_0)^2 - 2\frac{(1 - \cos\phi_0)}{\beta \cdot a}(a \cdot t_0) + \frac{1}{a^2} = 0 \tag{6}$$

which can be solved analytically or numerically. The root we are looking for is the one with real value which provides $t_0 < 1$. Finally, the phase of the transmission zero can be related to bandwidth by:

$$\phi_0 = \frac{2\pi}{2\sqrt{2}} \cdot \frac{\lambda_c^{\,2}}{c_0} \frac{\Delta f}{FSR} \quad \text{or} \quad \phi_0 = \frac{2\pi}{2\sqrt{2}} \cdot \frac{\Delta f}{fsr} \tag{7}$$

where λ_c is the central wavelength of the switch, Δf is the bandwidth or flat region where the through port transmission is smaller than the ripple (β), c_0 is the light speed at vacuum, FSR is the Free Spectral Range in wavelength domain and fsr is the Free Spectral Range in frequency

#117101 - $15.00 USD Received 11 Sep 2009; revised 12 Nov 2009; accepted 16 Nov 2009; published 23 Nov 2009

domain. Therefore, once the values of Δf, β and a are specified, one can determine the transmission for each directional coupler present in the device. It can be demonstrated from the equations above that, for devices with losses, one can have a box-like transfer function only if the value of ϕ_0 is greater than a minimum value ϕ_{min}:

$$\phi_{\min} = \frac{2\cdot\left(a^4 + a^2\right) - \beta\cdot\left(a^6 + a^4 + a^2 + 1\right)}{2\cdot\left(1-\beta\right)\cdot\left(a^4 + a^2\right)} \tag{8}$$

3. Fabrication, experimental description and results

The process flow of the structure ensures that the diodes are electrically isolated for independent tuning of each cavity, an important requirement to achieve hitless operation. We fabricate the device on a silicon-on-insulator (SOI) substrate with a 250 nm device layer on a 3 μm buried oxide layer. Waveguides and cavities are created by patterning and etching 210 nm of the 250 nm top silicon layer, leaving a 40 nm slab throughout the chip. The diodes are made by doping the slab regions around each cavity. We achieve electrical isolation by etching the silicon slab in undoped regions including between the cavities. The hard mask used for patterning the waveguides and cavities protects them in this etching step, while additional patterned HSQ resist is used as a mask for the remaining slab regions. Although only one of the cavities requires dynamic tuning, we create electrical contacts to both cavities in order to fine tune the device spectra if needed. Restricting a slab to the cavity region improves both optical coupling at the tapered chip input and propagation losses through the waveguide. The quasi-TM propagation mode is chosen for this study because it has lower dependence on sidewall roughness as compared to the quasi-TE mode, usually providing a cleaner spectrum. The shape of the device was designed to be equivalent to a racetrack in the region where a strong coupling is required and equivalent to a ring in the coupling region where the coupling is weak, therefore allowing waveguides to be placed further apart and reducing mode conversion losses [22]. For a device with power ripple of 17.5 dB below the transmission, bandwidth of 60 GHz and losses about 10 dB/cm we obtain coupling parameters $t_0 = 0.811$, $t_1 = 0.970$ and $t_2 = 0.800$ which were achieved using spacings of 304 nm, 350 nm and 300 nm, and linear region lengths of 3797 nm, 673 nm and 3797 nm, respectively. The fabrication of the PIN structure is performed by implanting BF_2^+ and As as acceptor and donor dopants, respectively, with a $10^{19}cm^{-3}$ concentration for both [23]. Nickel silicide is formed for contacting the doped regions, and aluminum is used for the contact pads. A Scanning Electron Microscope picture of the cavities with doped Silicon slab surrounding them is shown in Fig. 3(a), an Optical Microscope picture of the device before evaporating the Aluminum pads is shown in Fig. 3(b). The measured spectrum of the device fabricated is shown in Fig. 3(c).

#117101 - $15.00 USD Received 11 Sep 2009; revised 12 Nov 2009; accepted 16 Nov 2009; published 23 Nov 2009

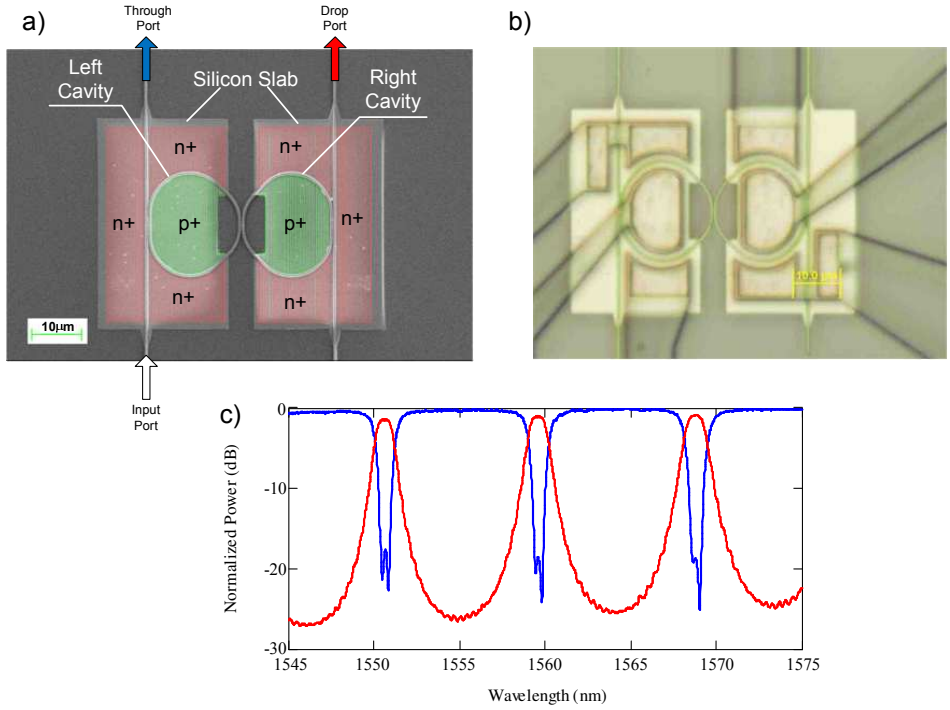

Fig. 3. (a) SEM picture of the device with the p^+ (green) and n^+ (red) implanted areas highlighted. The Si waveguides have 250 nm x 450 nm cross-section. The device is clad with 1 μm of silicon dioxide and has a 3 μm silicon dioxide BOX. Each cavity has a total length $2\pi \cdot 10$ μm with 8 μm bend radius. (b) Optical microscope picture of the device before evaporating aluminum for contact pads. (c) Spectrum of the fabricated device without any carrier injection.

Broadband hitless switching behavior is demonstrated by measuring the dynamics of the spectrum as the switch is turned ON and OFF. We monitor the output power at the through and drop ports during both carrier injection and extraction on an oscilloscope with a 30 GHz bandwidth optical sampling module. We scan the input laser from 1547.3 nm to 1554.3 nm with steps of 0.05 nm and observe the spectrum dynamics shown in Fig. 4.

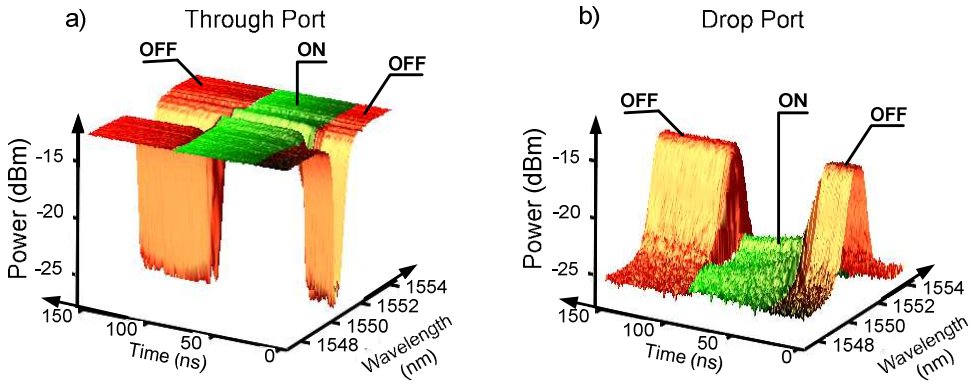

Fig. 4. (a) Dynamics of the spectrum for the through port. Switch starts in OFF state (red), it is turned ON at 15 ns (green) and is turned OFF again at 110 ns (red). (b) Dynamics of the spectrum for the drop port. Notice that the box-like spectrum disappears in the period where the switch is kept ON.

#117101 - $15.00 USD Received 11 Sep 2009; revised 12 Nov 2009; accepted 16 Nov 2009; published 23 Nov 2009

The switching times of the device, free-carrier concentration and amount of refractive index change are obtained by fitting the measured data to the theoretical model. We simulate the device behavior by plugging the refractive index change and losses in the transfer function equations of the device [Eqs. (1) to (3)]. In order to obtain the relation between refractive index change and current applied, a DC experiment is performed to separate the blue shift in the resonance, given by free-carrier concentration [24], from the slow red shift provided by thermal effect [25,26]. The influence of the temperature and carrier concentration on the device performance are distinguishable when a DC bias is applied by approximating the carrier concentration as directly proportional to the current and the device temperature as proportional to the power dissipated (or the current squared):

$$\Delta n_{eff} = -c_1 I + c_2 I^2 \tag{9}$$

where Δn_{eff} is the change in effective refractive index, and c_1 and c_2 are proportionality constants. In order to measure the resonance shift carefully, we apply a DC voltage to the cavity coupled to the input waveguide and measure both the maximum resonance shift ($\Delta\lambda_{DCmax}$) and the current that provides this shift (I_{DCmax}). Using the relationship $\Delta n_{eff} / n_g = \Delta\lambda / \lambda$, Eq. (9) becomes:

$$\Delta n_{eff} = -\left[\frac{2n_g}{\lambda}\right]\cdot\left[\frac{\Delta\lambda_{DC\max}}{I_{\max}}\right] I + \left[\frac{n_g}{\lambda}\right]\cdot\left[\frac{\Delta\lambda_{DC\max}}{I_{\max}^2}\right] I^2, \tag{10}$$

where n_g is the group index and λ is the original resonance wavelength. Equation (10) provides a direct relation between index change and current flowing through the device, from which we obtain the free carrier concentration as a function of the current. This procedure allows us to identify the term with I^2 dependence and suppress it from the model simulated for device operation much faster than the time constants of the thermal effect. We extract the free-carrier concentration inside the device from the free-carrier concentration index change (Δn_{Si}) and free-carrier absorption losses ($\Delta\alpha$) dependence of silicon, given by [24,27,28]:

$$\Delta n_{Si} = -8.8\times10^{-22} N - 8.5\times10^{-18} P^{0.8},\ [N]=[P]=cm^{-3} \tag{11}$$

$$\Delta\alpha = 8.5\times10^{-18} N + 6.0\times10^{-18} P,\ [\Delta\alpha]=cm^{-1} \tag{12}$$

where Δn_{Si} is the index change of the silicon waveguide for a given concentration of electrons (N) and holes (P). The index change in the silicon is related to the overall index change, by the confinement factor (Γ) of the field, which in our case is Γ = 0.81 [29]. Once Δn_{Si} is known and $N = P$ in the steady state, we obtain the free carrier concentration as a function of the current. The losses added to the right cavity ($\Delta\alpha$) are obtained from the Eq. (12), which closes the set of variables used in the modeling. In Figs. 5 and 6 we show simulated (continuous lines) and measured (dotted lines) spectrum (Fig. 5) and time response (Fig. 6) for the through (blue) and drop (red) ports. The drop port transmission changes by 9.8 dB when the switch is turned ON with a 1.46 V bias and 4.0 Vpp switching signal. The through port transmission has an ON/OFF ratio of 16.6 dB. When the device is ON, the right cavity has a 2.8 nm resonance shift meaning an index change Δn_{eff} = 0.009 and a free carrier density around $3.6\text{x}10^{18}$ cm^{-3}. The contact resistance of the device is R_S = 437 Ω and the power consumed in ON state considering a 0.7 V junction potential is 17.4 mW. The time domain signal for a single wavelength at 1550.8 nm is shown in Fig. 6(a). In Fig. 6(b) we show the result of switching a 1 Gbps modulated signal with central wavelength 1550.8 nm. Figure 7(a) shows the eye diagram of a 10 Gbps signal input. Figure 7(b) shows the same signal at the drop port. We notice that the 60 GHz bandwidth accommodates the 10 Gbps signal with low distortion. By fitting the simulated curve to the experimental resuts when a DC voltage is applied we estimate $\Delta\lambda_{DCmax}$ = 0.8 nm with I_{DCmax} = 2.0 mA. Plugging these values in Eq. (10) and

#117101 - $15.00 USD Received 11 Sep 2009; revised 12 Nov 2009; accepted 16 Nov 2009; published 23 Nov 2009

considering that the thermal effect is negligible for the dynamics of the system we obtain, for a *1/e* amplitude decay, the time constants for the switch as 7 ns for OFF-ON transition and 3 ns for ON-OFF transition.

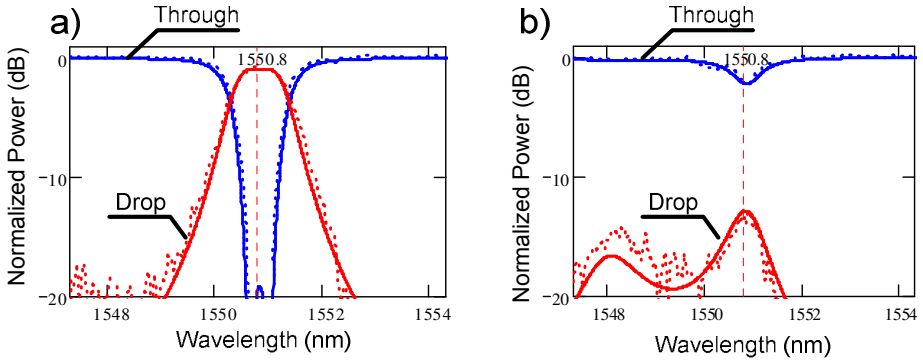

Fig. 5. (a) Instantaneous spectrum for the switch off at 10 ns. (b) Instantaneous spectrum for the switch on at 107.5 ns Dotted lines represent experimental data while continuous lines are the calculated values.

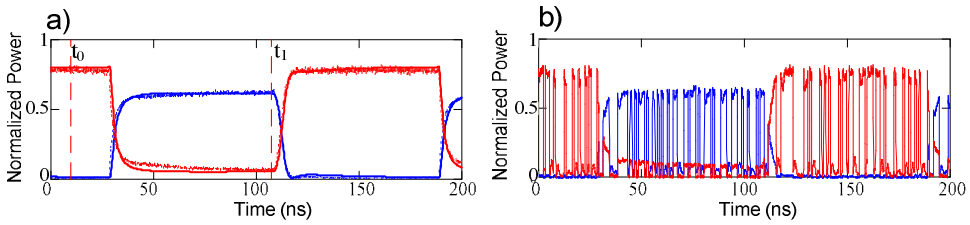

Fig. 6. (a) Time domain response for a single 1550.8 nm wavelength as input. Experimental result is shown in dotted lines, while result from fitting is shown in continuous line; (b) time domain for a 1 GHz modulated signal as input.

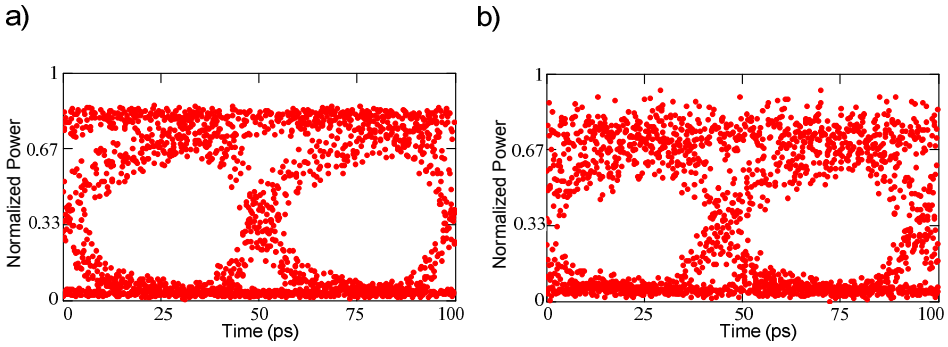

Fig. 7. Eye diagram of a 10 Gbps signal (a) at input and (b) at drop port.

We demonstrate, as can be seen in Fig. 6, that at least an 80 ns window can be sustained with the switch ON with a 7 ns transient time. For a 10 Gbps signal going through the device it represents switching of up to 710 bits. Note that the holding time and current applied (i.e. the extinction ratio) are not independent, being necessary to reduce the current when longer holding times are required. In fact we are able to hold the device for more than 1 μs for extinction ratios 4 dB smaller than the values shown in Fig. 5. Longer hold times, essential for

#117101 - $15.00 USD Received 11 Sep 2009; revised 12 Nov 2009; accepted 16 Nov 2009; published 23 Nov 2009

on-chip networks, can be achieved using novel electro-optic structures [30], or reducing the surface recombination rates [31].

4. Operational limits

The extinction ratio experienced by each port when the switch goes from OFF state to ON state is limited by the maximum current that the diode can tolerate. Destructive experiments with the fabricated diodes shows that DC currents around 7 mA can damage them, limiting the detuning we can provide for the switch. For a resonant cavity, the maximum optical detuning needed for maximum extinction ratio is

$$\Delta n_{MAX} = \frac{\lambda}{4\pi R}. \tag{13}$$

For this amount of refractive index change, the detuned cavity needs to have its resonance shifted by half FSR of the device, which corresponds to 4.5 nm for the switch demonstrated here. To avoid damaging the device, we limit the current to 6.3 mA and obtain at most a 2.8 nm detuning. Even though 2.8 nm detuning is only 62% of the maximum detuning, its effect in the ON/OFF ratio is much stronger: for the drop port, the 9.8 dB ON/OFF ratio obtained experimentally represents 79% of the theoretical value for maximum detuning; for the through port, the 16.6 dB ON/OFF ratio obtained experimentally represents 98% of the theoretical value for the maximum detuning. Both values agree with the theoretical result for a 2.8 nm detuning, which also shows that reasonable ON/OFF ratios can be obtained much before the maximum detuning is achieved.

The insertion loss for this switch topology has to be considered for drop and through ports in three main points: the central wavelength in the drop port when the switch is OFF, the central wavelength in the through port when the switch is ON and the detuned wavelength in the through port when the switch is ON. An illustration of these points is indicated in Fig. 9 as A, B and C, and, for the device fabricated, we obtained 0.5 dB, 2.0 dB and 0.4 dB, respectively. The insertion losses are a function of the synthesis parameters (bandwidth and ripple) and intrinsic losses of the device. Point B shows an over-coupled resonance, which can cause residual dispersion at this resonance. Simulations performed show a lorentzian delay with a 10 ps peak at the central wavelength. This delay in a system with many switches cascaded might require dispersion compensation or a slight detuning of the spectrum relative to the central wavelength to ensure low signal distortion.

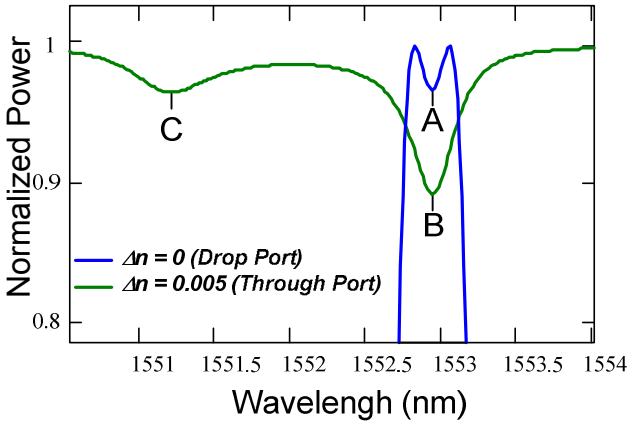

Fig. 9. Insertion losses of the switch. Spectrum shows the insertion losses for A. the drop port insertion loss when the switch is OFF, B. the through port insertion loss at the central wavelength when the switch is ON And C. The through port insertion loss at the detuned wavelength when the switch is ON.

#117101 - $15.00 USD Received 11 Sep 2009; revised 12 Nov 2009; accepted 16 Nov 2009; published 23 Nov 2009

5. Conclusion

We show the characteristics of a broadband (60 GHz), spectrally hitless, compact (20 μm x 40 μm), fast (7ns) electro-optical switch. The device, composed of two coupled resonant cavities, has independently addressable PIN diodes, and the hitless behavior happens when only the cavity connected to the output waveguide is detuned by free-carrier injection. Thermal effects in the device limit the hold time to about 80 ns, and the fabricated device shows an ON/OFF extinction ratio of 9.8 dB for the drop port and 16.6 dB for the through port when driven by a 1.46 V bias and 4.0 Vpp switching signal, with total power consumption of 17.4 mW. This demonstrated device is a critical component for on-chip networks.

Acknowledgment

This work was performed in part at the Cornell NanoScale Facility, a member of the National Nanotechnology Infrastructure Network, which is supported by the National Science Foundation (Grant ECS-0335765). This work was partly supported by the Air Force Office of Scientific Research with Grant FA9550-07-1-0200 under the supervision of Dr. Gernot Pomrenke, and by the National Science Foundation (NSF) under Career Grant No. 0446571. Hugo Lira thanks sponsorship support provided by the Brazilian Defense Ministry.

#117101 - $15.00 USD Received 11 Sep 2009; revised 12 Nov 2009; accepted 16 Nov 2009; published 23 Nov 2009